Eur. Phys. J. B (2012) 85: 366
DOI: 10.1140/epjb/e2012-30430-6

THE EUROPEAN PHYSICAL JOURNAL B

Regular Article

In situ measurements of ultimate bending strength of CuO and ZnO nanowires

B. Polyakov[1,2,a], L.M. Dorogin[1], S. Vlassov[1], M. Antsov[1], P. Kulis[2], I. Kink[1,3], and R. Lohmus[1]

[1] Institute of Physics, University of Tartu, Riia st. 142, 51014 Tartu, Estonia
[2] Institute of Solid State Physics, University of Latvia, Kengaraga st. 8, LV-1063 Riga, Latvia
[3] Estonian Nanotechnology Competence Centre, Riia 142, 51014 Tartu, Estonia

Received 30 May 2012 / Received in final form 9 July 2012
Published online 8 November 2012 –

Abstract. Young's modulus and the bending strength of copper oxide and zinc oxide nanowires (NWs) were measured in situ using nanomanipulation techniques inside a scanning electron microscope (SEM). Young's modulus was measured by bending half-suspended NWs and simultaneously measuring the force using a sensor based on a quartz tuning fork. Bending strength was measured for the NWs on a flat surface by bending them from one end with an AFM tip until the NW broke. The profile of the elastically deformed NW and the average value of Young's modulus were used to calculate the bending strength of the NWs. Weibull statistics was applied to analyse and compare the bending strength distribution for NWs made from both materials.

1 Introduction

One-dimensional solids such as nanowires (NWs) and nanotubes (NTs) exhibit many unique properties that make them candidates for numerous future nanoscale devices and applications. The small length scale of NWs allows them to be grown as dislocation-free heterostructures. This architecture was demonstrated in the pioneering works of Lieber et al. [1,2] for axial GaAs/GaP and radial core-shell GaN/InGaN/AlGaN NWs and Samuelson et al. [3] for InAs/InP NWs.

As is well known from fracture mechanics, the ultimate strength of a brittle material is inversely proportional to the square root of the size of critical structural defects randomly distributed in the volume of material [4]. A small concentration of defect and self-purification effects (ability to expel impurities) are directly linked to the extremely high mechanical strength of NWs, which can approach their theoretical strength [5].

Considering the extraordinary mechanical properties of semiconducting NWs, it is necessary to also mention the strong piezoresistive or piezoelectric effects discovered in some nanostructured materials. For example, He and Yang reported giant piezoresistive properties of Si NWs [6], and Wang described the outstanding piezoelectric properties of ZnO NWs [7].

Nanoelectromechanical systems (NEMS) based on NW or NT materials possess a Young's modulus of up to a few hundred GPa, a small mass and a high ultimate strength, and they can be operated at frequencies in the GHz or THz range. Moreover, in contrast to carbon NTs, semiconducting NWs have predictable electrical properties and can be easily combined with conventional semiconductor technologies. Knowledge about the mechanical properties of NWs will help in the design and engineering of the next generation of NEMS and will contribute to a better understanding of nanoscale mechanics.

Young's modulus is a characteristic parameter that determines the behaviour of NWs during nanomanipulations; if Young's modulus is known, many other parameters can be found (e.g. bending strength; static and kinetic friction parameters [8–11]). Many methods have been developed to measure Young's modulus and the ultimate strength of NWs or NTs. The most popular of these methods utilise ambient atomic force microscopy (AFM). The method of vertical loading of a nanowire suspended over either a hole or a trench has been applied to investigate the mechanical properties of Ge, ZnO, and other NWs [12,13]. More sophisticated methods, such as lateral loading of NWs, were demonstrated for SiC and CNT by Wong et al. [14]. A serious drawback of AFM-based methods is the lack of visual control during experiments.

Another simple method of determining Young's modulus, which was applied for ZnO and GaN NWs [15,16], is the excitation of mechanical oscillations in a NW fixed at one end and measuring its resonance response by sweeping the excitation frequency during observation with either a transmission electron microscope (TEM) [17] or a scanning electron microscope (SEM).

Young's modulus can also be determined by contact mode atomic force microscopy (AFM), in which one end of the NW is fixed on the edge of a rigid substrate. The elastic

[a] e-mail: boris.polyakov@cfi.lu.lv

deformation force is calculated from the lateral deformation of the NW against a calibrated AFM cantilever inside the SEM or TEM [18]. Axial loading or stretching of a NW glued between a rigid substrate and a calibrated AFM cantilever was applied to investigate Si and B NWs, as well as CNTs [19–22]. In all of these methods the NWs or NTs under investigation are either glued or fixed by focused ion beam assisted deposition. Barth et al. demonstrated an advanced method for the real-time measurement of Young's modulus and ultimate strength by using a vertically grown array of SnO_2 NWs in an SEM combined with contact-mode AFM [23].

In the work reported here, a force sensor made by gluing an AFM tip to a quartz tuning fork (QTF) was used to dynamically measure Young's modulus and the ultimate strength of a half-suspended NW. The measurements were made in situ using a scanning electron microscope. This experimental setup benefits from a compact design and an adjustable force sensitivity range that is not limited by a cantilever force constant. In a related experiment, the ultimate strength of NWs adhered to a flat substrate was measured using the elastic bending of a NW pushed from one end by an AFM tip, where the NW itself works as a force sensor [9].

This study was focused on investigation of mechanical properties of ZnO and CuO NWs. Both materials can be easily synthesized in form of superior quality NWs, and these materials are expected to be used for optoelectronic and photovoltaic applications [24,25]. Even being brittle in bulk form materials, they become extremely elastic at the nanoscale as e.g. NWs. ZnO NWs having hexagonal crystalline structure possess piezoelectric properties, which in combination of high elasticity make NWs unique material for various nanoelectromechanical devices [7]. CuO NWs have monoclinic crystalline structure. Rich application potential of CuO NWs is not fully explored yet. Copper atoms have very high diffusion rate; copper have several oxidation states (Cu_2O, CuO), and easily can be reduced back to metallic copper, which open routes for synthesis of sophisticated nanoscale architectures [26].

Usually, information on the mechanical properties of different nanostructured materials (e.g., ultimate strength) cannot be directly compared because of the different approaches used by different research groups. Here, the same methods were used to investigate CuO and ZnO NWs; this approach allows their mechanical properties to be directly compared.

2 Materials and methods

2.1 Nanowires

ZnO NWs were grown by a vapour transport method using Au nanoparticles (BBI international, 60 nm) as catalysts [27]. NWs were grown on silicon substrates by heating a 1:4 mixture of ZnO and graphite powder to 800−900 °C in an open-end quartz tube for 30 min. Synthesised NWs were a few tens of μm long, with diameters in the range of 50 to 200 nm.

CuO NWs were grown by heating copper foil at 400 °C in an open-ended quartz tube over a period of two hours [28]. Synthesised NWs were 10−20 μm long, with diameters in the range of 30 to 150 nm.

High-resolution SEM observations revealed that the dominant cross-section of the NWs is hexagonal and rectangular for ZnO and CuO NWs, respectively.

After growth, the NWs were transferred onto substrates. A large fraction of the NWs were broken into shorter wires (several microns long) during the transfer process.

2.2 Young's modulus measurements on half suspended nanowires

For Young's modulus measurements, either a square patterned calibration grating (NT-MDT TGX1, period 3 μm, height 0.6 μm) or a silicon wafer with trenches fabricated by focused ion beam (FIB) were used as substrates [8]. NWs with one end suspended over the trench and another end fixed to the substrate surface by either a strong adhesive or forces of static friction were used for the experiments. The measurements were based on the bending of the free end of a half-suspended NW by a sharp tip. Force was measured simultaneously with visual observation inside a SEM (Fig. 1a). The data were then fitted to a model from which Young's modulus was calculated.

The force sensor was made by gluing an AFM cantilever (*Nanosensor* AdvancedTEC-CONT) using conductive silver epoxy (*Agar Scientific*) to one prong of the QTF (*Elfa*, nominal resonance frequency at 32.768 kHz). The tip was glued so as to oscillate parallel to the sample surface and perpendicular to the NW. The tip was electrically connected to the QTF electrode to exclude charging effects. The QTF was driven at its resonant frequency, with typical values of the driving voltage in the range of 10−30 mV. The dependence of oscillation amplitude on the applied force (force sensitivity) of the QTF was measured on precalibrated cantilevers (FCL, *AppNano* and CSG11 $C = 0.03$−0.1 N/m, *NT-MDT*) using a procedure similar to that described in [29,30]. The signal from the QTF was amplified by a lock-in amplifier (SR830, *Stanford Research Systems*) and recorded through an ADC-DAC card (*National Instruments*).

The force sensor was mounted on a 3D nanomanipulator (SLC-1720-S, *SmarAct*) and installed inside the SEM (Vega-II SBU, *TESCAN*), which operates at a typical chamber vacuum of 3×10^{-4} mbar. Special software was developed to control the nanomanipulator and record simultaneous signals from the nanomanipulator's position sensors and from the lock-in amplifier. A more detailed description can be found in our previous articles [8,31].

2.3 Bending strength measurements on a flat substrate

NWs were deposited onto silicon wafers (Fig. 1b) for bending strength measurements on a flat substrate. No force

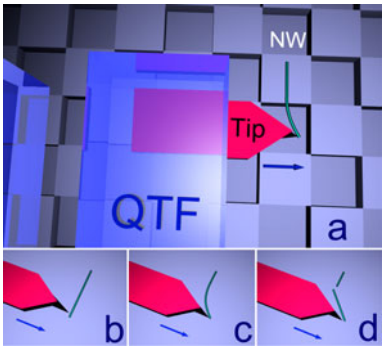

Fig. 1. (Color online) Schematics of in situ SEM experiments. Arrows indicate the direction of tip movement. Young's modulus measurement of a half-suspended NW pushed by an AFM tip glued on one prong of the QTF (a). Ultimate strength measurement for a NW adhered to a flat substrate and pushed by the AFM tip (b-d).

registration was used. Standard contact mode AFM cantilevers (Nanosensor AdvancedTEC-CONT cantilevers; force constant 0.2 N/m; nominal tip radius, 10 nm) were connected directly to the nanomanipulator. The geometry of the cantilevers enabled tip visibility from above. The remaining set-up was the same as described in Section 2.2. The procedure consisted of bending the NW from one end while the other end stayed fixed to the substrate by strong adhesion/static friction, until breakage occurred. An average value of Young's modulus was used to calculate the stresses inside the NW based on its profile just before breaking (Fig. 1c). In more details this method is described in [9,11].

2.4 Model

To model the elastic bending of the NW in the measurement of both Young's modulus and bending strength experiments, we used the equation for the equilibrium of a bent elastic beam with Young's modulus E and momentum of inertia I loaded by a point force f at its end. This equation can be written as [32]:

$$EI\frac{d^2\theta}{dl^2} + f\cos\theta = 0, \tag{1}$$

where l is the natural axis of the NW and θ is the angle between the tangent of the bent profile and the initial straight profile of the NW. The equation can either be solved numerically or expressed in elliptic functions with the boundary conditions:

$$\theta|_{l=0} = 0, \tag{2a}$$

$$\left.\frac{d\theta}{dl}\right|_{l=L} = 0. \tag{2b}$$

Equation (2a) implies that the NW is fixed along its axis in the adhered part, and equation (2b) is dictated by the absence of momentum at the end of the NW. The maximal tensile stress $\sigma_{\max}$ that apparently occurs on the outermost side of the NW can be expressed as:

$$\sigma_{\max} = ED\kappa/2, \tag{3}$$

where κ is local curvature of the NW defined as $\kappa = d\theta/dl$ and D is diameter of the NW. Given these relationships, the following parameters of a bent NW with a given geometry can be distinguished: Young's modulus E, the loading force f, and the NW profile $\theta(l)$. Knowing any 2 of the parameters is sufficient for determining the state of the bent NW and the calculation of the maximal tensile stress.

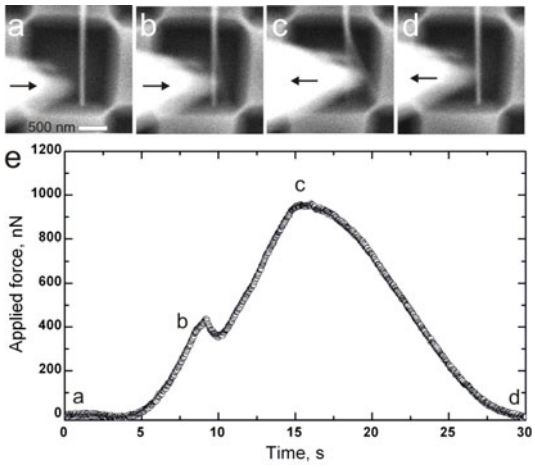

Fig. 2. Real-time measurement of Young's modulus of a half-suspended NW. Arrows indicate direction of tip movement. Sequence of SEM images of CuO NW bending (a)–(d) and the corresponding force curve during linear loading of NW (e); Young's modulus was calculated to be $E = 222$ GPa.

3 Results and discussion

3.1 Measurements of Young's modulus

Figure 2 shows several snapshots of a typical set of Young's modulus measurements and their corresponding force curves. The suspended part of the NW was gradually bent by the AFM tip (Figs. 2a–2c). The AFM tip looks blurred because of the oscillation of the QTF. After contact with the tip, the NW oscillates at the QTF frequency. Only the extreme positions of the NW that have zero speed are visible (Figs. 2b–2c). Increasing the elastic force generated inside of the bent NW causes a gradual increase in the force detected by the QTF (Fig. 2e). When the tip moves backward and detaches from the NW, the force signal registered by the QTF is restored to its initial value (Fig. 2d). The QTF amplitude signal (proportional to the applied force) and the sequence of SEM images of the gradually bent NW were recorded simultaneously during the experiment. The value of Young's modulus was numerically calculated using equation (1) by overlaying the beam profile on the SEM image of the bent NW while the applied force was registered by the QTF.

Our previous measurements indicated that the static friction force for both ZnO and CuO NWs is very high [8,9,11]. For example, shear stress of CuO NWs on smooth substrate is around 1 GPa [11], and NW-substrate contact area of 100×100 nm^2 provides stiction sufficient to withstand applied force of 10^4 nN. In our Young modulus measurement experiments typical values of applied force were 1000−2000 nN and NWs contact area 100×1000 nm^2, providing enough force to strongly fix NW during loading experiment. Due to this fact no additional fixing (e.g., by FIB assisted deposition [18] or by evaporation of material through a shadow mask [14]) is needed, which significantly simplifies the method.

Measurements were carried out on 9 CuO NWs, resulting in values ranging from 30 to 400 GPa with an average value of 204 ± 116 GPa. These results are presented graphically in Figure 5a. Our values are in good agreement with the only available literature data reported by Tan et al. [33], in which Young's modulus of CuO NWs was measured by performing a three-point bend test with an AFM and found to be in the range of 70 to 300 GPa. Large variations in the modulus were explained by the existence of outer amorphous layers of various thicknesses.

Young's modulus measured for 14 ZnO NWs ranged from 22 to 117 GPa. The statistics of the measurements for the individual NWs are presented in Figure 5b. The average value is 58 ± 34 GPa, which is in a good agreement with other works, such as those of Manoharan et al. [18] (40 GPa), Song et al. [34] (29 GPa), and Huang et al. [35] (58 GPa). Some other researchers found significantly higher value of ZnO NWs Young modulus; in details this problem is discussed in work of Rohlig et al. [13].

Nanowires are observed only from above in our experiment, making impossible the detection of any deviations in cross-sections from an ideal hexagon for ZnO NWs and square for CuO NWs. However, a small inaccuracy in the determination of diameter and cross-section geometry results in significant errors in the calculations of Young's modulus and can contribute to a wide distribution of the obtained data. Rotation of the sample relative to the electron beam is required to increase the precision of the NW cross-section measurements; however, such rotation was not possible in our setup. As it was mentioned above, NW is strongly fixed to substrate by adhesion and static friction forces; possible uncertainty of coordinate l where starts the fixed region of NW is rather small and corresponding uncertainty in length of suspended part of NW does not contribute any significant error into Young modulus calculation.

3.2 Measurements of bending strength

Many of the bending experiments described in Section 3.1 exceeded the bending strength of the CuO NWs, which were therefore broken as a result of high stress; however, for broken NWs, it is still possible to measure the bending strength in addition to Young's modulus. Maximal stress is generated at the boundary between the motionless and suspended parts of the NW. A typical experiment

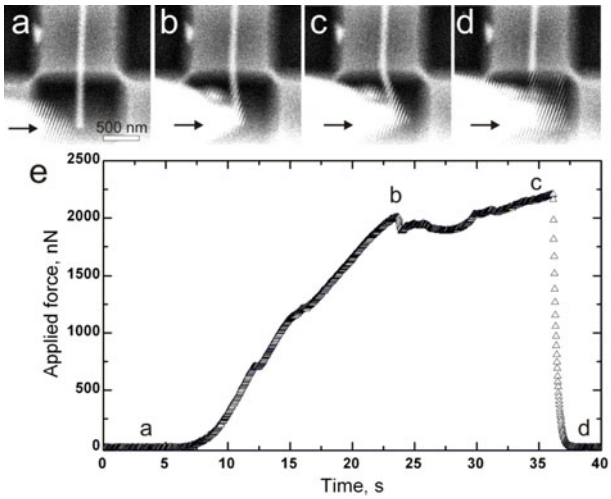

Fig. 3. Real-time measurement of the bending strength of a half-suspended NW. Arrows indicate the direction of tip movement. Sequence of SEM images of bent and broken CuO NW (a)−(d) and the corresponding force curve (e); Young's modulus was calculated to be $E = 130$ GPa, and the bending strength was calculated to be 16.7 GPa.

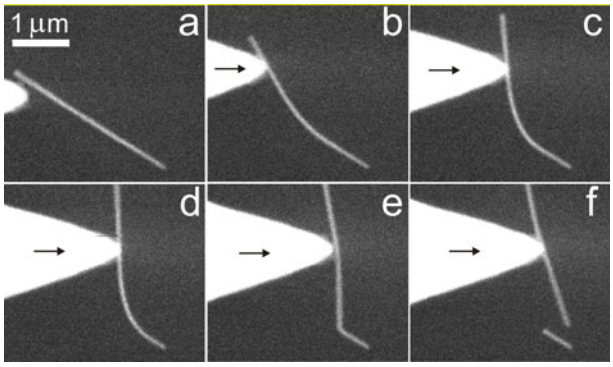

Fig. 4. Measurement of bending strength on a flat substrate. Arrows indicate the direction of tip movement. Intact CuO NW (a). Pushing one end of the NW by AFM tip (b)−(d). Maximal elastic bending of the NW before breaking (d). NW broken (e). Broken part moved forward (f). The calculated bending strength is 8.6 GPa.

is presented in Figures 3a−3d. Only the linear region of the loading curve, which corresponds to elastic bending of the NW (until $t = 24$ s, Fig. 3e), can be used to calculate Young's modulus. For larger bending angles, the force curve becomes nonlinear, the deformation is no longer elastic, and the NW ultimately breaks (at $t = 36$ s).

No breaking was observed for ZnO NWs. An alternative method of measuring the bending strength can be applied by considering the known Young's modulus. The NW on the flat substrate is pushed from one end by the standard AFM tip, and the evolution of the bending profile is monitored via the SEM. At the moment when the bending strength is exceeded, the NW breaks (Figs. 1c and 4d). In this case, the profile and Young's modulus serve as 2 independent parameters for the maximal tensile stress calculations described in paragraph 2.4. An average value of

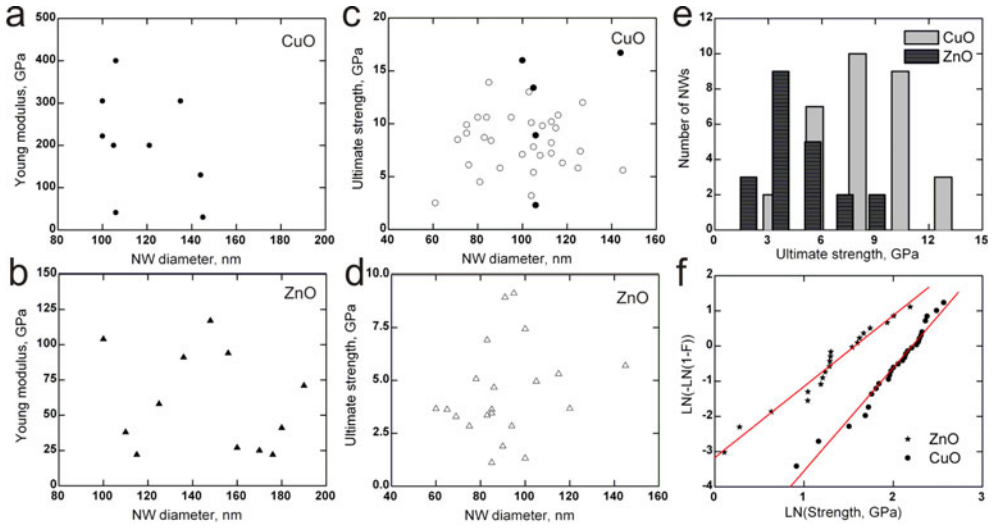

Fig. 5. (Color online) Statistics of Young's modulus and ultimate strength measurements of CuO and ZnO NWs. Young's moduli of CuO (a) and ZnO (b) NWs. Ultimate strength of CuO (c) and ZnO (d) NWs. Corresponding histograms of ultimate strength (e) and Weibull plots for CuO and ZnO NWs (f).

Young's modulus was used to fit the actual profile of the maximally bent NW. This method is significantly simpler in comparison to that previously described because no external force sensor is needed.

Bending strength was measured for 31 CuO NWs on a flat substrate (Fig. 5c, hollow circles) and for 5 half suspended NWs using a QTF force sensor (solid circles). The results obtained by both methods are consistent. Similar measurements of the bending strength for 21 ZnO NWs are shown in Figure 5d. The average bending strengths of CuO and ZnO NWs are 8.2 ± 2.7 GPa and 4.4 ± 2.2 GPa, respectively. For convenient comparison of the experimental data, the results are also plotted in the form of histograms (Fig. 5e).

The strength of materials is mostly determined by the statistical distribution of structural defects inside the material. For ceramics and other brittle materials, the maximal stress that a sample can withstand before failure may vary from specimen to specimen, even under identical testing conditions. It is also known that the strength of a brittle material decreases as its size increases [36]. Thus, nanoscale materials generally have significantly higher strength values in comparison to bulk materials as a result of their considerably lower defect content. At the same time, the distribution of defects in nanostructures is more random. As a result, the strength variation from specimen to specimen for nanoscale materials increases.

The strength distribution is often described by Weibull statistics, which was successfully applied for carbon and MoS_2 nanotubes and ZnO nanowires [36,37]. The probability of failure for a specimen at an applied stress σ is

$$F(\sigma) = 1 - \exp\left[-\left(\frac{\sigma}{\sigma_0}\right)^m\right], \quad (4)$$

where σ_0 is the characteristic strength (i.e., the stress at which 63% of the specimens have failed), and m is the Weibull modulus (also called the shape parameter). The Weibull modulus is a dimensionless parameter of the Weibull distribution used to describe variability in the measured strength of brittle materials. Higher m values correspond to a steeper Weibull plot and indicate a lower dispersion of fracture stresses.

The Weibull plot for both CuO and ZnO NWs is shown in Figure 5f. The Weibull moduli are $m \approx 2$ for ZnO and $m \approx 3$ for CuO. Characteristic strengths of $\sigma_0 = 6.5$ GPa for CuO and $\sigma_0 = 3.2$ GPa for ZnO were obtained. These values are comparable to the moduli $m = 1.7$ and $m = 2.4$ found by Barber et al. [37] for chemical vapour deposition and arc discharge synthesised multiwall carbon NTs. Lu [36] reported values of $m = 5.7$ and $\sigma_0 = 7.41$ GPa for ZnO NWs, indicating higher strength and less variation in comparison to our samples. It can be concluded that CuO NWs demonstrate significantly higher strength and lower data scatter than ZnO. This result may indicate that CuO NWs have a more uniform structure and defect distribution.

For bulk materials the experimental values of strength are always much smaller (orders of magnitude) than the theoretical values, which can be approximately estimated as $\sigma_{theor} = E/2\pi$ [38]. For nanoscale materials the experimental strength can approach the theoretical strength limit. The theoretical strength of CuO and ZnO NWs was calculated using average values of their Young's modulus and yielded 33 GPa and 9.2 GPa, respectively. Comparing the experimentally measured bending strength of the NWs with their theoretical strength yields 20% of the theoretical value for CuO and 35% for ZnO.

4 Conclusions

In situ nanomanipulation techniques were used to determine Young's modulus and the bending strength of CuO and ZnO NWs. Weibull statistics was applied to analyse the distribution of bending strength values. Weibull

moduli of $m \approx 2$ for ZnO and $m \approx 3$ for CuO NWs were obtained. Characteristic strengths of $\sigma_0 = 6.5$ GPa for CuO and $\sigma_0 = 3.2$ GPa for ZnO NWs were obtained, corresponding to 20% and 35% of their theoretical strengths, respectively.

P.K. was supported by ESF Grant No. 2009/0202/1DP/1.1.1.2.0/09/APIA/VIAA/141. B.P. was supported by the Estonian Science Foundation (ETF grant JD162), ESF FANAS program "Nanoparma" and European Union through the European Regional Development Fund (Centre of Excellence "Mesosystems: Theory and Applications", TK114). The work was also partly supported by ETF grants 8420, 9007 and Estonian Nanotechnology Competence Centre (EU29996).

References

1. M.S. Gudiksen, L.J. Lauhon, J. Wang, D.C. Smith, C.M. Lieber, Nature **415**, 617 (2002)
2. F. Qian, S. Gradecak, Y. Li, C.-Y. Wen, C.M. Lieber, Nano Lett. **5**, 2287 (2005)
3. L. Samuelson, M.T. Bjork, K. Deppert, M. Larsson, B.J. Ohlsson, N. Panev, A.I. Persson, N. Skold, C. Thelander, L.R. Wallenberg, Physica E **21**, 560 (2004)
4. B.R. Lawn, in *Fracture of Brittle Solids*, 2nd edn. (Cambridge University Press, Cambridge, 1993)
5. W. Hao, J. Li, H. Xu, J. Wang, T. Wang, ACS Appl. Mater. Int. **2**, 2053 (2010)
6. R. He, P. Yang, Nat. Nanotechnol. **1**, 42 (2006)
7. Z. Wang, Nano Today **5**, 540 (2010)
8. B. Polyakov, L. Dorogin, S. Vlassov, I. Kink, A. Lohmus, A. Romanov, R. Lohmus, Solid State Commun. **151**, 1244 (2011)
9. B. Polyakov, L. Dorogin, S. Vlassov, I. Kink, A. Romanov, R. Lohmus, Micron **43**, 1140 (2012)
10. L.M. Dorogin, B. Polyakov, A. Petruhins, S. Vlassov, R. Lohmus, I. Kink, A.E. Romanov, J. Mater. Res. **27**, 580 (2012)
11. B. Polyakov, S. Vlassov, L. Dorogin, P. Kulis, I. Kink, R. Lohmus, Surf. Sci. **606**, 1393 (2012)
12. L.T. Ngo, D. Almecija, J.E. Sader, B. Daly, N. Petkov, J.D. Holmes, D. Erts, J.J. Boland, Nano Lett. **6**, 2964 (2006)
13. C.-C. Rohlig, M. Niebelschutz, K. Brueckner, K. Tonisch, O. Ambacher, V. Cimalla, Phys. Status Solidi B **247**, 2557 (2010)
14. E. Wong, P. Sheehan, C. Lieber, Science **277**, 1971 (1997)
15. Y. Huang, X. Bai, Y. Zhang, J. Phys.: Condens. Matter **18**, L179 (2006)
16. C.-Y. Nam, P. Jaroenapibal, D.Tham, D.E. Luzzi, S. Evoy, J.E. Fischer, Nano Lett. **6**, 153 (2006)
17. R. Lõhmus, D. Erts, A. Lõhmus, K. Saal, J. Jompol, H. Olin, Phys. Low-Dim. Struct. **3**, 81 (2001)
18. M. Manoharan, A. Desai, G. Neely, M. Haque, J. Nanomater., doi:10.1155/2008/849745 (2008)
19. M. Yu, B. Files, S. Arepalli, R. Ruoff, Phys. Rev. Lett. **84**, 5552 (2000)
20. Y. Zhu, F.Xu, Q. Qin, W. Fung, W. Lu, Nano Lett. **9**, 3934 (2009)
21. C. Hsin, W. Mai, Y. Gu, Y. Gao, C. Huang, Y. Liu, L. Chen, Z. Wang, Adv. Mater. **20**, 3919 (2008)
22. C. Lin, H. Ni, X. Wang, M. Chang, Y. Chao, J. Deka, X. Li, Small **6**, 927 (2010)
23. S. Barth, C. Harnagea, S. Mathur, F. Rosei, Nanotechnol. **20**, 115705 (2009)
24. G. Filipic, U. Cvelbar, Nanotechnology **23**, 194001 (2012)
25. Z. Zhu, T. Chen, Y. Gu, J. Warren, R. Osgood Jr., Chem. Mater. **17**, 4227 (2005)
26. Y. Qin, Y. Yang, R. Scholz, E. Pippel, X. Lu, M. Knez, Nano Lett. **11**, 2503 (2011)
27. M. Huang, Y. Wu, H. Feick, N. Tran, E. Weber, P. Yang, Adv. Mater. **13**, 113 (2001)
28. X. Jiang, T. Herricks, Y. Xia, Nano Lett. **2**, 1333 (2002)
29. C. Su, L. Huang, K. Kjoller, Ultramicrosc. **100**, 233 (2004)
30. S. Fain Jr., K. Barry, M. Bush, B. Pittenger, R. Louie, Appl. Phys. Lett. **76**, 930 (2000)
31. S. Vlassov, B. Polyakov, L. Dorogin, A. Lõhmus, A. Romanov, I. Kink, E. Gnecco, R. Lõhmus, Solid State Commun. **151**, 688 (2011)
32. L. Landau, E. Lifshitz, in *Theory of Elasticity*, 3rd edn. (Butterworth-Heinemann, Oxford, 1986)
33. E. Tan, Y. Zhu, T. Yu, L. Dai, C. Sow, V.C. Tan, C. Lim, Appl. Phys. Lett. **90**, 163112 (2007)
34. J. Song, X.Wang, E. Riedo, Z. Wang, Nano Lett. **5**, 1954 (2005)
35. Y. Huang, X. Bai, Y. Zhang, J. Phys.: Condens. Matter. **18**, 179 (2006)
36. Ch. Lu, Phys. Lett. A **372**, 6113 (2008)
37. A.H. Barber, I. Kaplan-Ashiri, S.R. Cohen, R. Tenne, H.D. Wagner, Compos. Sci. Technol. **65**, 2380 (2005)
38. C.R. Barrett, W.D. Nix, A.S. Tetelman, in *The Principles of Engineering Materials*, edited by E. Cliffs and N.J. Prentice Hall (Prentice Hall, New Jersey, 1973)